Bioactive Materials 6 (2021) 4717–4728

Contents lists available at ScienceDirect

Bioactive Materials

journal homepage: www.sciencedirect.com/journal/bioactive-materials

Injectable and thermosensitive hydrogels mediating a universal macromolecular contrast agent with radiopacity for noninvasive imaging of deep tissues

Xiaohui Wu [a], Xin Wang [a], Xiaobin Chen [a], Xiaowei Yang [a], Qian Ma [a], Guohua Xu [b], Lin Yu [a,c,*], Jiandong Ding [a,c]

[a] State Key Laboratory of Molecular Engineering of Polymers, Department of Macromolecular Science, Shanghai Stomatological Hospital, Fudan University, Shanghai, 200438, China
[b] Department of Orthopedic Surgery, Spine Center, Changzheng Hospital, Naval Medical University, Shanghai, 200003, China
[c] Zhuhai Fudan Innovation Institute, Zhuhai, Guangdong, 519000, China

ARTICLE INFO

Keywords:
Thermosensitive hydrogels
Radiopacity
Block copolymers
In vivo degradation
Non-invasive deep tissue imaging

ABSTRACT

It is very challenging to visualize implantable medical devices made of biodegradable polymers in deep tissues. Herein, we designed a novel macromolecular contrast agent with ultrahigh radiopacity (iodinate content > 50%) via polymerizing an iodinated trimethylene carbonate monomer into the two ends of poly(ethylene glycol) (PEG). A set of thermosensitive and biodegradable polyester-PEG-polyester triblock copolymers with varied polyester compositions synthesized by us, which were soluble in water at room temperature and could spontaneously form hydrogels at body temperature, were selected as the demonstration materials. The addition of macromolecular contrast agent did not obviously compromise the injectability and thermogelation properties of polymeric hydrogels, but conferred them with excellent X-ray opacity, enabling visualization of the hydrogels at clinically relevant depths through X-ray fluoroscopy or Micro-CT. In a mouse model, the 3D morphology of the radiopaque hydrogels after injection into different target sites was visible using Micro-CT imaging, and their injection volume could be accurately obtained. Furthermore, the subcutaneous degradation process of a radiopaque hydrogel could be non-invasively monitored in a real-time and quantitative manner. In particular, the corrected degradation curve based on Micro-CT imaging well matched with the degradation profile of virgin polymer hydrogel determined by the gravimetric method. These findings indicate that the macromolecular contrast agent has good universality for the construction of various radiopaque polymer hydrogels, and can nondestructively trace and quantify their degradation *in vivo*. Meanwhile, the present methodology developed by us affords a platform technology for deep tissue imaging of polymeric materials.

1. Introduction

Non-invasive *in vivo* bioimaging techniques have emerged a vital impact on modern medical practice and greatly promote advances in a variety of biomedical applications, such as *in vivo* cell labeling, early disease diagnosis, image-guided treatment and post-operative medical devices follow-up [1–4]. In particular, X-ray fluoroscopy has been utilized in clinic for more than a century and has the advantages of low-cost, high spatial resolution and unrestricted depth of tissue penetration [5,6]. X-ray computed tomography (CT) imaging is also based on the absorption of X-rays and has the ability to visualize three dimensional (3D) morphology of implanted objects/devices [5,7].

Since the beginning of the new century, many permanent implantable devices for various disease treatments have been gradually replaced by biodegradable devices made of polymeric materials [8–11]. Nevertheless, polymeric materials are usually transparent to X-rays due to the atomistic composition of C, H, O, and N atoms. To nondestructively locate these devices/materials, trace morphology changes, and quantify the *in situ* degradation profiles, contrast agents are generally required.

Peer review under responsibility of KeAi Communications Co., Ltd.
* Corresponding author. State Key Laboratory of Molecular Engineering of Polymers, Department of Macromolecular Science, Shanghai Stomatological Hospital, Fudan University, Shanghai, 200438, China.
E-mail address: yu_lin@fudan.edu.cn (L. Yu).

https://doi.org/10.1016/j.bioactmat.2021.05.013
Received 7 April 2021; Received in revised form 26 April 2021; Accepted 8 May 2021

One conventional approach to endow polymers with X-ray opacity is to blend X-ray absorbing additives, such as metal powders, barium salts, zirconium dioxide, organic iodine compounds, *etc* [12–15]. However, this method suffers from some important defects: (1) the physical, chemical and mechanical properties of polymeric materials are often influenced due to the incorporation of fillers [15]; (2) it is not easy to blend small-molecule contrast agents evenly with polymers; (3) small-molecule contrast agents easily leach and penetrate into body fluids, resulting in the loss of X-ray opacity and causing systemic toxicities [7,13,14]. An attractive alternative is to develop macromolecular radiographic contrast agents by covalently modifying a radiocontrast probe, typically an iodine-containing moiety, to the polymer skeleton, thereby overcoming the drawbacks of small-molecule contrast agents [6,16,17].

In-situ-forming injectable hydrogels as implantable biomaterials/devices have attracted tremendous attention because of their minimally invasive administration mode [18–30]. In particular, thermosensitive and biodegradable hydrogels comprised of copolymers of hydrophobic polyesters, such as poly(lactic acid) (PLA), poly(ε-caprolactone) (PCL), poly(lactic acid-*co*-glycolic acid) (PLGA), poly(ε-caprolactone-*co*-glycolic acid) (PCGA), poly(ε-caprolactone-*co*-lactic acid) (PCLA), and hydrophilic poly(ethylene glycol) (PEG) are free-flowing polymer aqueous solutions at low or ambient temperature; however, they exhibit sol-gel transitions in response to the changes in temperature [31–36]. Bioactive substances and live cells are then easily loaded by blending them with a low viscous polymer solution and this loading process thoroughly avoids contact with organic solvents. After injection into the target site of a warmblooded animal, a substance/cell-containing hydrogel is spontaneously formed via the temperature-triggered gelation, acting as a reservoir of drugs or a cell-growing matrix. Meanwhile, *in-situ* gelation also affords a perfect match for filling a complex defect. In virtue of the characteristics of facile synthesis, good biocompatibility and adjustable biodegradability, thermosensitive PEG/polyester copolymer hydrogels have suggested for various applications in biomedical fields, such as drug delivery [35,37–42], wound repair [43], tissue regeneration [44,45] and post-surgical anti-adhesion [34,46].

As a kind of implantable and biodegradable biomaterials, nondestructive and real-time monitoring of thermosensitive hydrogels at the injection sites as well as acquirement of information on *in vivo* behaviors of degradation are of significance for their fundamental research and following clinical translation. However, there are few reports on the PEG/polyester thermosensitive hydrogels for X-ray imaging modalities so far. The first PEG/polyester polymer thermosensitive hydrogel with X-ray opacity was developed by our group [47], where 2,3,5-triiodobenzoic acid (TIB) as a radiocontrast dye was covalently modified to the hydrophobic end of methoxy poly (ethylene glycol) (mPEG)-PLA diblock copolymer and the aqueous solution of TIB-capped mPEG-PLA with a very narrow PEG/PLA ratio window could form a temperature-responsive hydrogel. This methodology could not be employed to obtain other types of radiopaque and thermosensitive hydrogels. For example, temperature-responsive hydrogels composed of ABA-type polyester-PEG-polyester or BAB-type mPEG-polyester-mPEG triblock copolymers are more popular compared with thermosensitive mPEG-polyester diblock copolymers. However, due to thermosensitive polyester-PEG-polyester triblock copolymers featuring a subtle end-group effect [48,49] plus the very strong hydrophobicity of TIB group, their TIB-capped derivatives only precipitated in water and failed to form a thermosensitive hydrogel [47]. As to thermosensitive mPEG-polyester-mPEG triblock copolymers, TIB cannot be covalently modified due to the lack of reactive groups.

Is there a method free of post-modification? We have taken this into account and made efforts to address this challenge. In this study, we designed an iodinated polycarbonate-based universal macromolecular contrast agent, poly(5,5-bis(iodomethyl)-1,3-dioxan-2-one)-*co*-poly(ethylene glycol)-*co*-poly(5,5-bis(iodomethyl)-1,3-dioxan-2-one) (PITMC-PEG-PITMC, PI), with ultrahigh radiopacity, as illustrated in Fig. 1. The molecular design of PI was mainly based on the following two considerations. First, since thermosensitive PEG/polyester copolymers that exhibit temperature-responsive sol-gel transitions in water are attributed to their amphiphilic nature [50–52], the

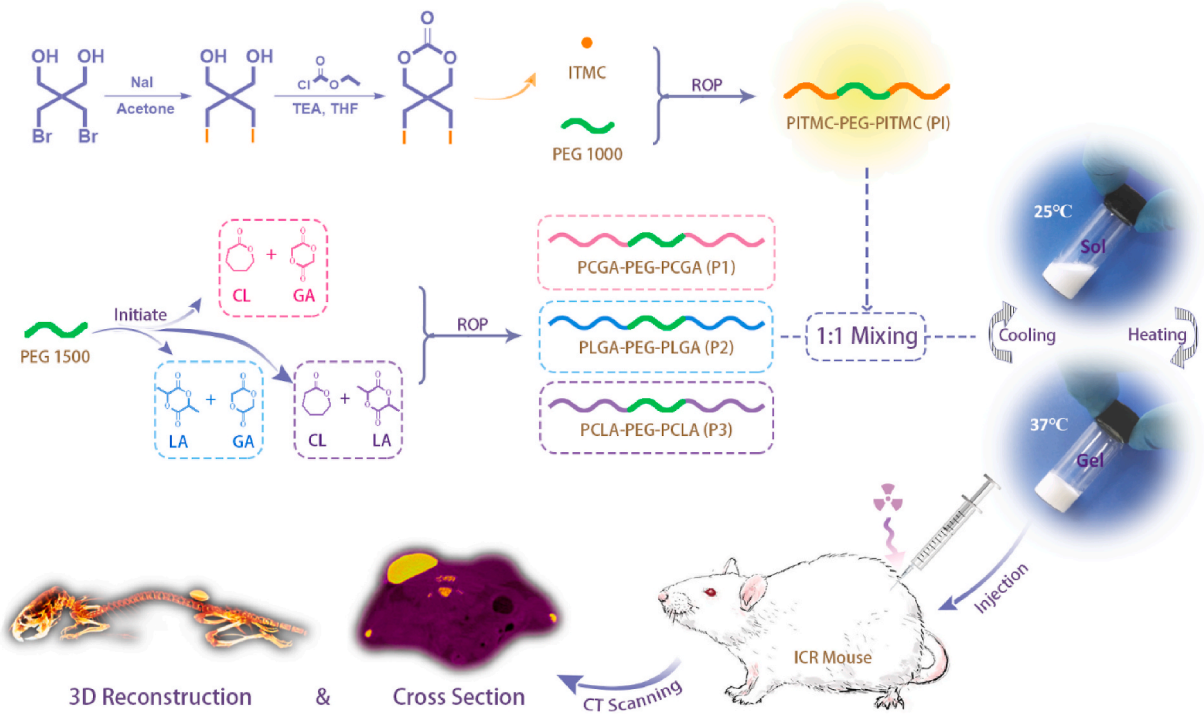

Fig. 1. Schematic presentation of design of macromolecular contrast agent, construction of radiopaque and thermosensitive PEG/polyester copolymer hydrogels, and their nondestructive imaging *in vivo* via Micro-CT. CL: ε-caprolactone, GA: glycolide, ITMC: 5,5-bis(iodomethyl)-1,3-dioxan-2-one, LA: D,L-lactide, PEG: poly(ethylene glycol), ROP: ring-opening polymerization, TEA: triethylamine, THF: tetrahydrofuran.

macromolecular radio-opacifier should be amphiphilic to facilitate mixing with them to form a homogeneous system and maintain the capacity of thermogelation. Second, to ensure the adequate iodine content in macromolecular radio-opacifier, the molecule weight (MW) of PEG should not be very high and eventually PEG with MW 1000 Da was selected by us. Meanwhile, a set of thermosensitive hydrogels comprised of polyester-PEG-polyester polymers with different, but familiar polyester compositions were chosen as the demonstration materials to validate the universality of macromolecular contrast agent for the fabrication of radiopaque and thermosensitive hydrogels, as presented in Fig. 1. The effect of the PI introduction on their thermogelation properties was evaluated. The imaging capacity of radiopaque hydrogels in deep tissues was tested *in vitro* and *in vivo*. Finally, the feasibility to nondestructively monitor and quantify hydrogel degradation *in vivo* was demonstrated.

2. Results and discussion

2.1. Synthesis and characterization of macromolecular contrast agent PI and polyester-PEG-polyester polymers

5,5-bis(iodomethyl)-1,3-dioxan-2-one (ITMC), a diiodinated carbonate monomer, was synthesized via iodine exchange reaction in the presence of 2,2-bis(bromomethyl)-1,3-propanediol and subsequently cyclization with ethyl chloroformate using triethylamine (TEA) as an acid scavenger, as presented in Fig. 1, and nuclear magnetic resonance hydrogen spectroscopy (^{1}H NMR) analysis confirmed the successful acquirement of ITMC monomer (Fig. S1). Then, a novel macromolecular contrast agent PI with excellent radiopacity was obtained via initiating macromolecular initiator PEG1000 to conduct ring-opening polymerization (ROP) of ITMC in the presence of zinc bis[bis(trimethylsilyl)amide] ($Zn(HMDS)_2$) as the catalyst. The chemical structure and composition of PI were analyzed by ^{1}H NMR, X-ray photoelectron spectroscopy (XPS), energy-dispersive X-ray spectroscopy (EDS) and gel permeation chromatography (GPC). As displayed in Fig. 2A, the characteristic proton peaks belonging to PI were clearly assicribed, and the average number of ITMC repeating units in each PI calculated by its ^{1}H NMR spectrum was 14.5. Namely, the iodine content in PI reached amazing 56.3 wt%, which is significantly superior to the known iodinated polyesters/polycarbonates [6,16,53–55], to the best of our knowledge. Different from PEG, except for the signals of carbon and oxygen elements, the strong signal of iodine element was also sucessfully detected on the surface of PI by XPS and EDS analysis (Fig. 2B and C and S2). The GPC trace of PI presented a unimodal pattern, as diplayed in Fig. S3. All these features demonstrated that the ROP was successfully conducted and the desired macromolecular contrast agent PI was harvested.

Meanwhile, three thermosensitive PEG/polyester triblock copolymers, poly(ε-caprolactone-*co*-glycolic acid)-*b*-poly(ethylene glycol)-*b*-poly(ε-caprolactone-*co*-glycolic acid) (PCGA-PEG-PCGA, P1), poly(lactic acid-*co*-glycolic acid)-*b*-poly(ethylene glycol)-*b*-poly(lactic acid-*co*-glycolic acid) (PLGA-PEG-PLGA, P2), poly(ε-caprolactone-*co*-lactic acid)-*b*-poly(ethylene glycol)-*b*-poly(ε-caprolactone-*co*-lactic acid) (PCLA-PEG-PCLA, P3), were prepared by ROP of different monomers using stannous octoate as the catalyst and PEG1500 as the macroinitiator (Fig. 1). As shown in Fig. S4 and S5, the chemical compositions and structures of P1, P2 and P3 were confirmed by ^{1}H NMR and GPC. Molecular parameters of PI, P1, P2 and P3 copolymers are summarized in Table 1.

Table 1
Molecular parameters of PI, P1, P2 and P3 polymers in this study.

Sample	M_n[a]	[M1]/[M2][b]	M_n[c]	$Đ_M$[c]
PI	2770-1000-2770	–	3870	1.64
P1	1800-1500-1800	2.3/1 (CL/GA)	5240	1.35
P2	1790-1500-1790	1.9/1 (LA/GA)	4270	1.24
P3	1820-1500-1820	2.5/1 (CL/LA)	5350	1.33

[a] M_n calculated from ^{1}H NMR.
[b] Repeating unit ratio in mol/mol calculated from ^{1}H NMR.
[c] M_n and $Đ_M$ measured via GPC.

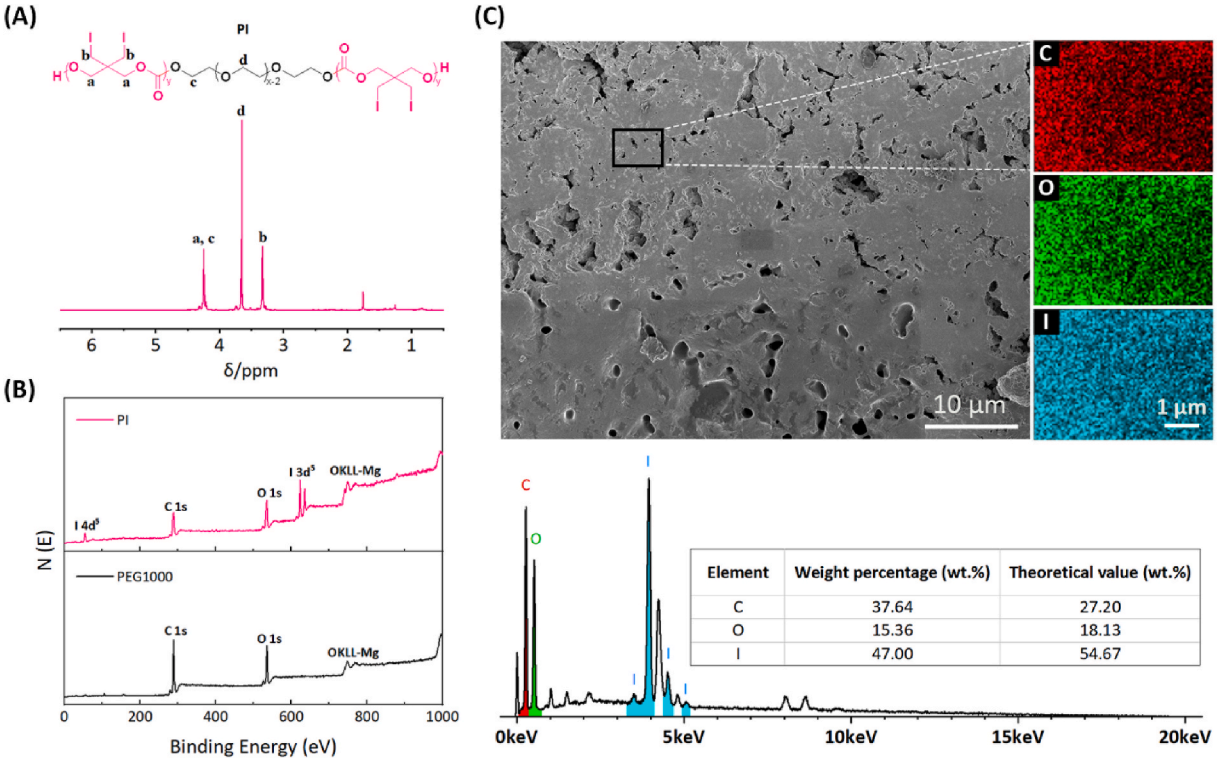

Fig. 2. Characterization of PI, the novel macromolecular contrast agent. (A) ^{1}H NMR spectrum of PI in $CDCl_3$. (B) Full XPS survey spectra for PI and PEG1000. (C) SEM image, EDS distribution maps and analysis results (wt%) for carbon (red dots), oxygen (green dots) and iodine (blue dots) of PI.

2.2. Sol-gel transitions of aqueous polymer solutions

All the three triblock copolymers, P1, P2 and P3, synthesized by our group could be dissolved in water to form low viscous sols at low or room temperature and exhibited a state transformation of sol-to-gel with responding to the environmental temperature increase when the polymer concentration was higher than the critical gel concentration (> 5 wt %). As illustrated in Fig. 3a, the 15 wt% aqueous polymer solutions were transparent at room temperature and formed opaque gels at body temperature. Our previous studies and others have demonstrated that amphiphilic PEG/polyester copolymers easily self-assemble in water to form core-corona micelles, which have a good capacity for solubilization of hydrophobic small-molecules or macromolecules [37,38,40,44,50,51]. In fact, the macromolecular contrast agent PI was so hydrophobic that it was only partially soluble in water. Fortunately, the aqueous solutions of thermosensitive P1, P2 and P3 polymers with suspended core-corona-like micelles were able to significantly solubilize the hydrophobic PI. After solubilization, the PI-loaded aqueous polymer solutions containing 30 wt% solute turned into a milky white state, but they were still uniform and easy to flow at room temperature and formed semi-solid gels at 37 °C (Fig. 3A), indicating that the incorporation of PI did not compromise the sol-gel transitions of the polymer solutions.

In order to further quantitatively evaluate the effect of PI introduction, changes in the storage modulus G' and loss modulus G'' of aqueous polymer solutions in the presence or absence of PI were observed as a function of temperature (Fig. 3B and S6). G' and G'' represent the elastic component and viscous component, respectively, of the system. Generally speaking, $G' < G''$ suggests the sol state of the system, while $G' > G''$ reflects the gel state [56,57]. Along with the elevation of temperature, both the G' and G'' of aqueous polymer solutions gradually increased and eventually the G' exceeded the G''. The temperature corresponding to the crossover point where G' and G'' are equal has be considered as the sol-gel transition temperature (T_{gel}) [56,57]. As shown in Fig. S6, all the three PI-free polymer aqueous solutions formed gels at about 32 °C due to their similar MWs, while the T_{gel}s of aqueous polymer solutions containing PI also remained around 32 °C (Fig. 3B). This finding further confirmed that the introduction of PI maintained the thermogelation properties of the virgin polymer solutions well.

2.3. In vitro X-ray opacity

First, to explore the relationship between iodine content and X-ray opacity, a series of aqueous solutions of iohexol, a commercially available iodine contrast agent, with indicated concentrations were prepared and then subjected to Micro-CT scanning. As shown in Fig. 4A, the grayscale indices and Hounsfield units of iohexol aqueous solutions were linearly positively correlated with the iodine content in the iohexol solution. The linear fitting equations were as follows:

$$Y1 = 9.37x + 16.91 \ (R^2 = 0.999) \quad (1)$$

$$Y2 = 241.27x - 2.35 \ (R^2 = 0.999) \quad (2)$$

where $Y1$ represents the grayscale index, $Y2$ means the Hounsfield unit, and x represents the iodine content (wt%).

According to Equations (1) and (2), the grayscale index and Hounsfield unit of a system can be conveniently calculated via its iodine content, and vice versa. It is worth pointing out that the difference in the preview of maximum absorption (P_{max}) can affect the grayscale index of the same sample. The larger the P_{max} is, the smaller the grayscale index of the material is, that is, P_{max} is inversely proportional to the grayscale index of the system. In contrast, the Hounsfield unit of a specimen is a fixed value.

In vitro X-ray opacities of the different aqueous polymer solutions were determined by Micro-CT. Due to the only presence of light atomic mass elements like C, H and O in P1–P3 polymers, their grayscale indices

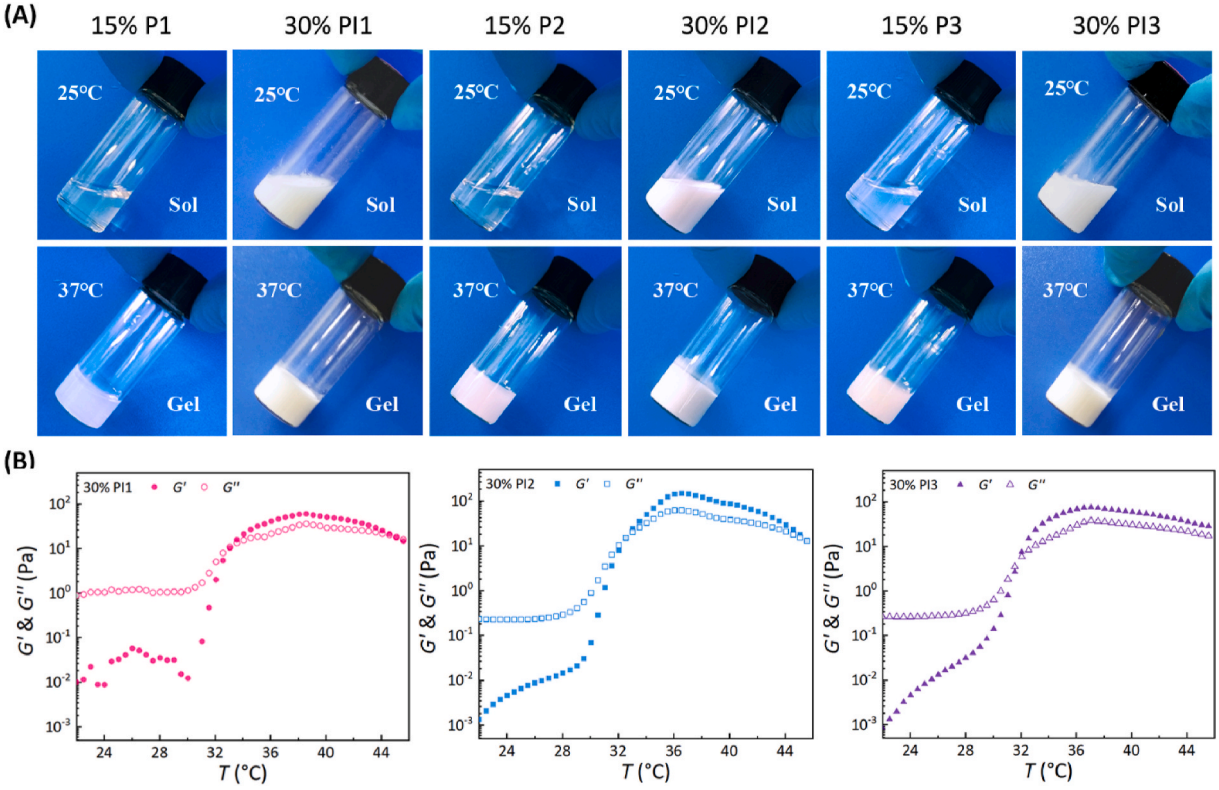

Fig. 3. Thermogelation behaviors of aqueous polymer solutions with or without the macromolecular contrast agent PI. (A) Photographs showing sol (25 °C) and gel (37 °C) states of the various aqueous polymer solutions. (B) Storage modulus G' and loss modulus G'' of the aqueous polymer solutions containing PI as a function of temperature. PI1 means the 1/1 (w/w) mixture of PI and P1, and the same is for PI2 and PI3.

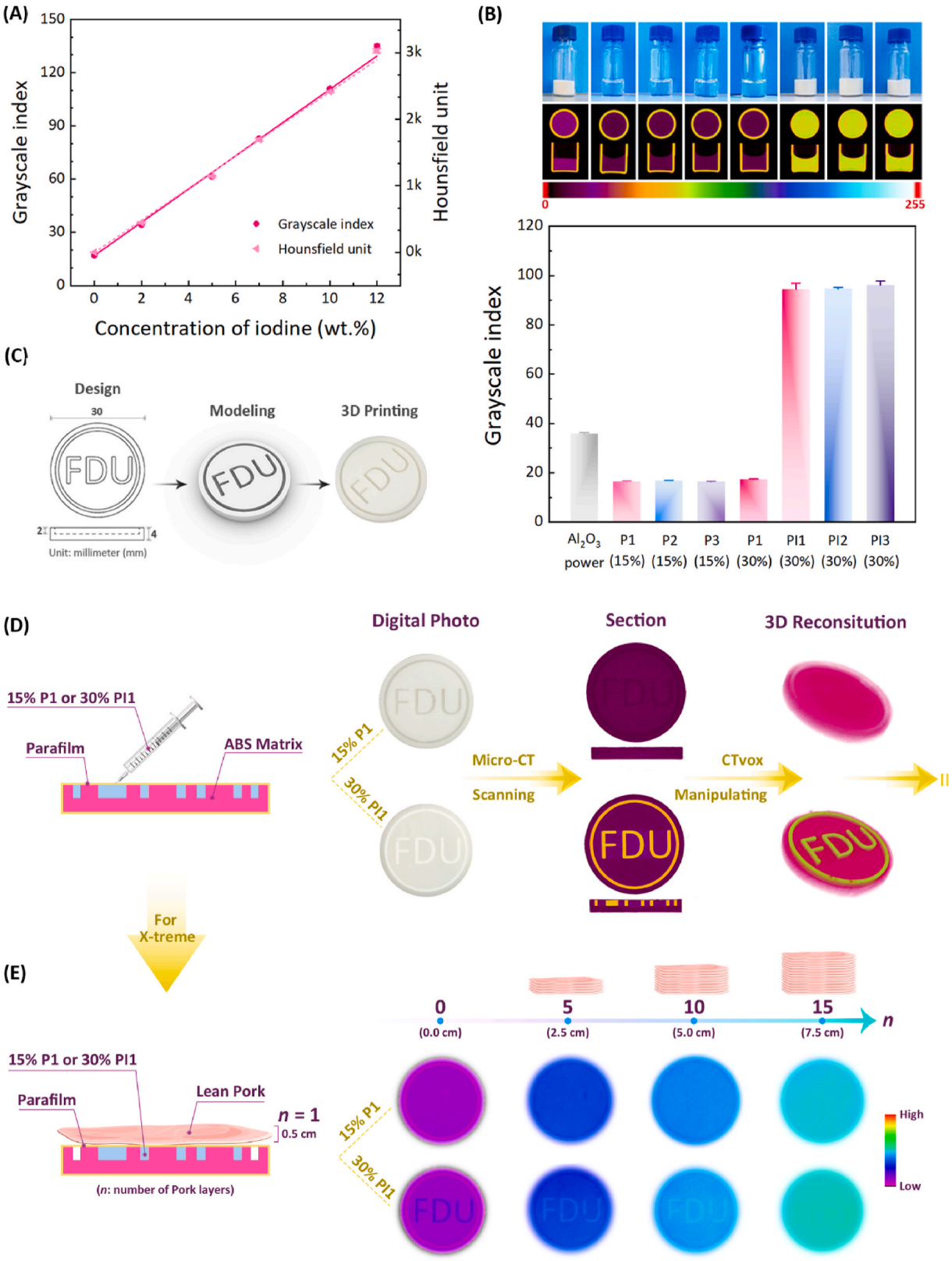

Fig. 4. X-ray opacity of various aqueous polymer solutions *in vitro*. (A) The linear relationship between the average grayscale indices/Hounsfield units of iohexol aqueous solutions and their iodine amounts ($n = 3$, $P_{max} = 0.1$). (B) The optical photographs, the corresponding Micro-CT images on the *x*-axis and the radiopacities of the indicated samples using the grayscale unit. The results are expressed as mean ± standard deviation (SD) ($n = 3$, $P_{max} = 0.1$). (C) Design, modeling and 3D printing of "FDU" pattern. (D) The X-ray opacity of "FDU" pattern containing P1 or PI1 solution using Micro-CT. (E) The X-ray opacity of "FDU" pattern containing P1 or PI1 solution covered with different layers of pork using X-treme.

of aqueous solutions were similar regardless of their structural composition and concentration, as presented in Fig. 4B. In contrast, the aqueous polymer solutions containing PI showed significantly enhanced radiopacity, and their grayscale indices increased to about 95, equivalent to the Hounsfield unit value of 2003, and were almost six times larger than those of the PI-free polymer solutions. Meanwhile, the radiopacities of the PI-loaded aqueous polymer solutions were also superior to that of the alumina powder as the control group and their grayscale indices were approximately 2.5 times that of alumina powder. The Hounsfield unit values of mineralized tissues such as bone are approximately 1000 [58]. Obviously, the radiopacities of the PI-loaded systems were twice those of mineralized tissues. In addition, the uniform distribution of grayscale as presented in Fig. 4B indicated that PI was effectively solubilized into the aqueous polymer solutions. Also, based on Equation (1) and the known grayscale indices of PI-loaded aqueous polymer solutions, the iodine content of PI could be calculated to be 55.4 wt%, equivalent to 13.3 ITMC repeating units in each PI, which was very close to the calculation result obtained from ^{1}H NMR.

To further visually demonstrate the X-ray opacity of PI-loaded aqueous polymer solutions, a 3D mold with "FDU" (abbreviation of Fudan University) pattern was designed and manufactured by 3D printing, whose detailed size parameters are illustrated in Fig. 4C. As shown in Fig. 4D, the "FDU" pattern filled with P1 solution was invisible under Micro-CT, while the pattern filled with PI1 solution could be clearly observed via Micro-CT imaging and the 3D reconstructed image intuitively reflected the morphology of the "FDU" pattern, indicating the outstanding X-ray opacity of PI1 system.

Similarly, the "FDU" pattern, which was filled with P1 solution, was not visualized under X-ray of X-treme, as shown in Fig. 4E. By contrast, due to the ultrahigh radiopacity of PI, the "FDU" pattern containing PI1 solution was still obviously visible through X-treme even when it was covered with 0.5 cm thick pork layer by layer to the 10th layer, and did not appear until the 15th layer was covered. It is worth noting that the X-ray imaging depth is proportional to the thickness and iodine content of the sample. The current "FDU" pattern contained only PI1 solution of 2 mm thickness, and the imaging depth has exceeded 5 cm. This finding affirms that the radiopaque PI1 system has an excellent capacity for deep tissue imaging. Of course, if the PI content in the polymer solution decreases, the imaging depth of the sample will decrease correspondingly.

2.4. *In vitro* cytotoxicity

The *in vitro* cytocompatibility of the polymers were tested by cell counting kit-8 (CCK-8) assay using normal mouse embryo osteoblast precursor cells (MC3T3-E1). As shown in Fig. 5, the viabilities of cells receiving the treatment of polymer mixtures, PI1, PI2 and PI3, for 24 h were as high as 90% at all the tested concentrations, which were similar to those treated with pure P1, P2 or P3 polymers (Fig. S7), indicating that the macromolecular contrast agent PI and the three PEG/polyester polymers have good cell compatibilities.

2.5. *In vivo Micro-CT imaging*

The different aqueous polymer solutions were injected subcutaneously into ICR mice through a conventional 1-mL syringe, and the *in situ*-forming hydrogels were obtained within 30 s via body temperature-triggered gelation, reflecting the appearance of elliptic protrusions at the administration sites. Subsequently, the *in vivo* X-ray opacities of *in situ*-forming hydrogels were evaluated by Micro-CT. Since the X-ray absorption capacity of pure polymer hydrogels without PI contrast agent was similar to that of soft tissue, it is impossible to distinguish them from the surrounding soft tissues using Micro-CT imaging, as shown in Fig. 6A. By contrast, with the mediation of excellent X-ray opacity of PI, the PI-loaded hydrogels could be visualized via Micro-CT with clear boundaries between the hydrogels and the adjacent soft tissues. Furthermore, the 3D morphologies of PI-loaded polymer hydrogels were intuitively observed by 3D

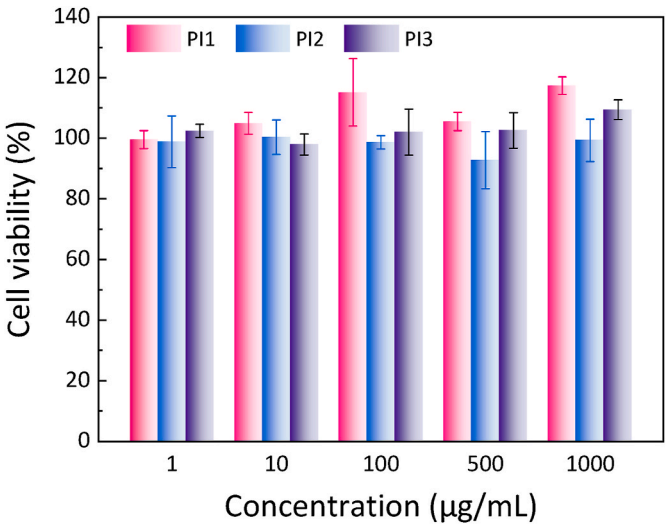

Fig. 5. *In vitro* cytotoxicity of the polymer mixtures, PI1, PI2 and PI3, as a function of polymer concentration against MC3T3-E1 cells. The viability of cells with the treatment of culture medium only was set as 100% and each point is represented as the mean ± SD (n = 4).

reconstruction of Micro-CT images (Fig. 6A and Video S1). The quantitative results of grayscale value and injection volume were also harvested. As presented in Fig. 6C and D, the three PI-loaded hydrogels had a similar grayscale index and injection volume. Their mean grayscale index was far greater than that of soft tissue; however, there was no obvious discrimination between the PI-free polymer hydrogels and the surrounding tissues. Meanwhile, the volume of PI-loaded hydrogels obtained from Micro-CT well coincided with the actual injection volume.

The three thermosensitive and radiopaque hydrogels were also intraperitoneally injected into ICR mice and then measured by Micro-CT. Fig. 6B displays their Micro-CT images on the z-axis and reconstructed 3D images. Likewise, these hydrogels were visible with the help of Micro-CT and exhibited an irregular shape, indicating that they were located in the space between the abdominal organs. The quantitative data validated that these hydrogels had prominently strong radiopacity compared with the adjacent abdominal organs (Fig. 6E). It should be noted that the intensity of X-ray opacity is related to the shape and injection site of the object tested. Owing to the more dispersed morphology of PI2 hydrogel in abdominal cavity compared with the other two hydrogels, its grayscale index was slightly lower than that of PI1 or PI3 hydrogel. Also, because the intraperitoneal injection site was deeper, the gray indices of these hydrogels were relatively smaller than those of subcutaneous injection. Moreover, these hydrogels had similar injection volume calculated by Micro-CT (Fig. 6F). These results indicate that PI is suitable as a universal macromolecular contrast agent for *in vivo* visualized detection of various thermosensitive hydrogels.

2.6. *Nondestructive monitoring of in vivo hydrogel degradation*

Considering that the medical applications of injectable thermosensitive hydrogels after subcutaneous injection are much more than those of intraperitoneal injection, the subcutaneous degradation process of PI1 hydrogel was nondestructively monitored by Micro-CT for example. Fig. 7A shows the volume and grayscale index of the residual PI1 hydrogel as a function of degradation time, and the morphological change of residual PI1 hydrogel over time is presented in Fig. 7B. The volume of the PI1 hydrogel gradually decreased as the time elapsed, whereas the remaining volume tended to be unchanged from day 24. The grayscale index of residual PI1 hydrogel showed a tendency to increase first and then slow decrease over time. In general, thermosensitive PEG/polyester copolymer hydrogels suffered from a rapid surface erosion by body fluids

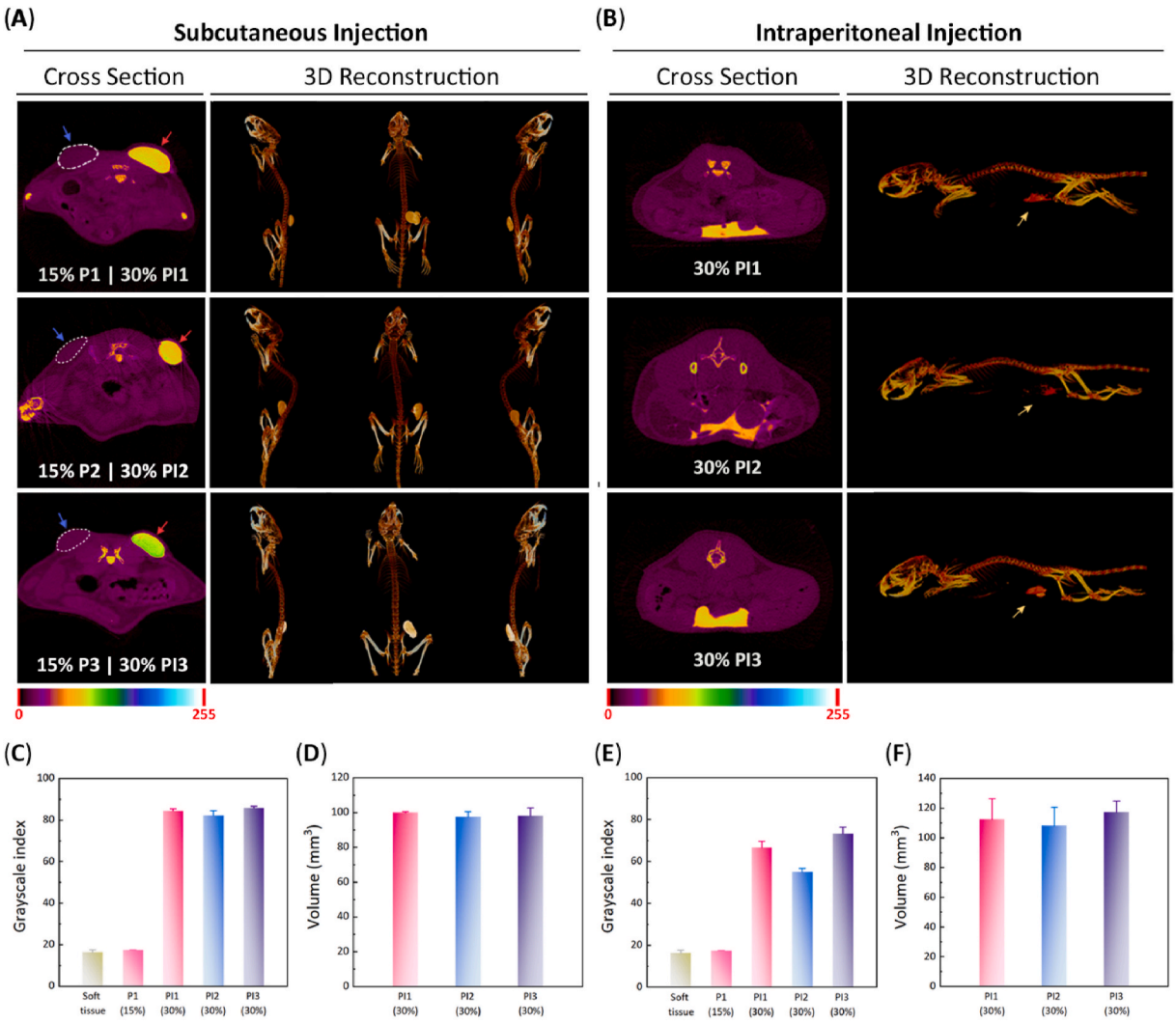

Fig. 6. (A) Cross-sectional views and 3D reconstructed Micro-CT images of the indicated samples 30 min after subcutaneous injection into female ICR mice. The dotted coils represent the PI-free hydrogels. (B) Cross-sectional views and 3D reconstructed Micro-CT images of the indicated samples 30 min after intraperitoneal injection into female ICR mice. (C) Grayscale indices of the indicated samples after subcutaneous injection. (D) Volume of the indicated samples after subcutaneous injection. (E) Grayscale indices of the indicated samples after intraperitoneal injection. (F) Volume of the indicated samples after intraperitoneal injection. ($n = 3$, $P_{max} = 0.1$).

at the first stage after subcutaneous injection, reflected by a significant reduction in gel vol/wt [32]. This feature was also observed in the current PI1 hydrogel. Because the macromolecular contrast agent PI was far more hydrophobic than thermosensitive P1 polymers, P1 polymers were more easily dissolved through body fluids in the first few days, resulting in an initial increase in the radiopacity of residual PI1 hydrogel.

To affirm that the degradation curve of the PI-mediated hydrogel did truly reflect the degradation process of PI-free polymeric hydrogel, a 15 wt% P1 aqueous solution was injected subcutaneously into ICR mice and then dissected for observation of degradation at the predetermined time points. As shown in Fig. 7C and D, the volume of the P1 hydrogel continuously decreased with the effluxion of time, and no residual gel was detected on day 33 post-injection, implying that it was almost completely degraded. Compared with the PI1 hydrogel, the pure P1 hydrogel without the macromolecular contrast agent PI seems to have a faster degradation rate. The previous studies have confirmed that the degradation rate of carbonate bonds is far lower than that of ester bonds [59–61]. Also, if the C–I bonds in PI break, iodide ions would be released, which should be diluted away immediately by body fluids. However, the residual PI1 hydrogel maintained strong radiopacity during the whole examination period, as demonstrated in Fig. 7A, indicating that the C–I bonds in PI should be stable and the remaining substance in the PI1 hydrogel on day 33 should belong to the undegradable macromolecular contrast agent PI. Therefore, the remaining volume of PI1 hydrogel on day 33 was used to correct the data of degradation at the previous time points one by one ($V_{33}' = V_{33} - V_{33}$; $V_{25}' = V_{25} - V_{33}$; $V_{19}' = V_{19} - V_{33}$ …) and then a new degradation curve was acquired. As displayed in Fig. 7D, the corrected degradation curve of PI1 hydrogel almost perfectly coincided with that of pure P1 hydrogel determined via the gravimetric approach. This finding convincingly demonstrates that PI as a macromolecular X-ray contrast agent can accurately and nondestructively quantify the *in vivo* degradation of the thermosensitive P1 hydrogel.

The ICR mice receiving the injection of the PI1 hydrogel were sacrificed, and then the main organs and adjacent tissues at the injection sites were harvested. The representative hematoxylin-eosin (H&E) staining slices of the main organs are shown in Fig. S8. Compared with normal organs, no significant abnormality was observed in the PI1 hydrogel group, suggesting that the injection of PI1 hydrogel and the subsequent degradation *in vivo* did not cause apparently systemic side effects. Fig. S9 displays the microphotograph of the subcutaneous tissue at the injection site and the corresponding CT scanning image of the

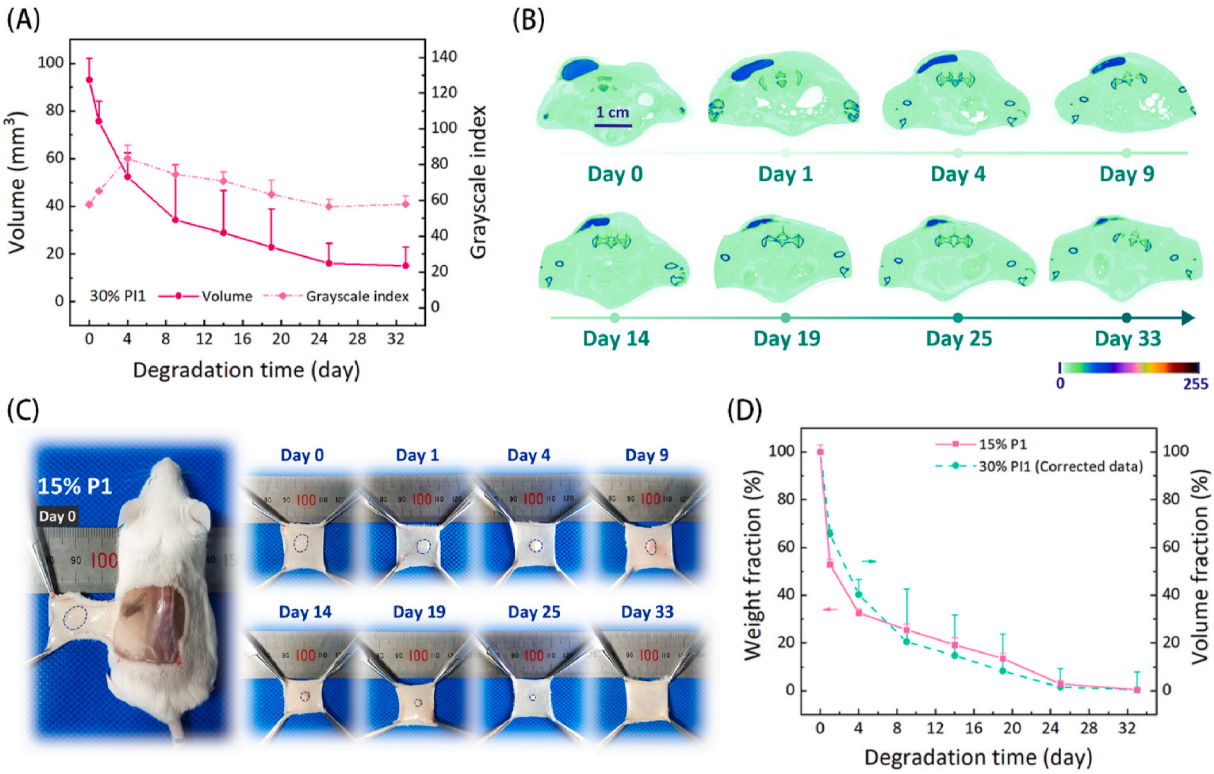

Fig. 7. The *in vivo* degradation of polymer hydrogels with or without the macromolecular contrast agent PI. (A) Changes in the volume and grayscale index of PI1 hydrogel over time after subcutaneous injection into female ICR mice. (B) Representative cross-sectional views of the remaining PI1 hydrogels at the predetermined time points. (C) Representative photographs of the remaining hydrogels in ICR mice that received the subcutaneous administration of 15 wt% P1 hydrogel. (D) Changes in the weight fraction of 15 wt% P1 hydrogel and the corrected volume fraction of 30 wt% PI1 hydrogel over time. The results are expressed as mean ± SD (n = 3).

paraffin-embedded tissue. A strong radiopaque signal at the injection site was still detected via Micro-CT. As mentioned above, the radiopaque signal should be attributed to the residual macromolecular contrast agent PI, which had not been degraded. Meanwhile, no obvious inflammatory reaction was observed around the residual gel, indicating that the macromolecular CT imaging agent PI has good biocompatibility *in vivo*.

3. Conclusions

By polymerizing ITMC functional monomers onto PEG, an ultrahigh radiopaque macromolecular contrast agent PI was designed and synthesized, which affords a universal contrast agent for the construction of radiopaque polymer hydrogels. The introduction of PI not only made all the hydrogels maintain temperature-responsive sol-gel transitions, but also provided the ability of radiopacity. The location, morphology and volume of the radiopaque hydrogels at different injection sites could be achieved via Micro-CT imaging nondestructively and accurately. The degradation profile determined by Micro-CT could truly reflect the *in vivo* fate of virgin polymer hydrogel. Except for the *in situ* monitoring of the *in vivo* degradation, the visualization of radiopaque thermosensitive hydrogels can facilitate their medical applications, such as embolization treatment, drug delivery, tissue regeneration, tissue marking, *etc*. Meanwhile, the current methodology can be easily extended to other implantable polymer devices for *in vivo* imaging at clinically relevant depths.

4. Experimental section

4.1. Materials

2,2-bis(bromomethyl)-1,3-propanediol, sodium iodide and sodium bisulfite were the products of Aladdin Biochemical Technology Co., Ltd. (Shanghai, China). Ethyl chloroformate was acquired from Wuhan Changcheng Chemical Technology Development Co., Ltd. (Wuhan, China). PEG1000 (number-average MW M_n = 1000 Da), PEG1500 (M_n = 1500 Da), $Zn(HMDS)_2$, stannous octoate and ε-caprolactone (CL) were bought from Sigma-Aldrich. Glycolide (GA) and D,L-lactide (LA) were acquired from Hangzhou Medzone Biotech Ltd. (Hangzhou, China). Iohexol was the product of TCI Development Co., Ltd. (Shanghai, China). Tetrahydrofuran (THF) and TEA were stirred in the presence of calcium hydride (CaH_2) for 24 h and then collected by distillation. CCK-8 for mammalian cells was bought from Beyotime Co., Ltd. (Shanghai, China). The other chemical reagents provided by Sinopharm Chemical Reagent Co. (Shanghai, China) were utilized without additional treatment.

4.2. Animals

Female ICR mice weighing approximately 25 g were purchased from Shanghai Lab. Animal Research Center (Shanghai, China). All animal experiments were conducted in accordance with the "Laboratory Animal Care Principles" (NIH Publication # 85–23, revised in 1985) and ratified by the Fudan University Ethics Committee.

4.3. Synthesis of ITMC

In according to our previous work [62], ITMC was synthesized via a two-step reaction. The first step of reaction was to synthesize 2,2-bis (iodomethyl)propane-1,3-diol. 30.0 g of 2,2-bis(bromomethyl)-1,3-propanediol (114.5 mmol), 60.0 g of sodium iodide (400.3 mmol) and 200 mL of acetone were transferred into an eggplant-shaped flask and a heating reflux was carried out for 8 days. Then, the filtrate obtained by filtering the generated sodium bromide, which was insoluble in acetone, was concentrated under reduced pressure to remove the solvent, and the

resulting mixture was washed with a 1% (w/v) aqueous sodium bisulfite solution (400 mL) to remove the iodine generated in the reaction. Finally, the desired diiodine-substituted compound was harvested via filtration and drying at 85 °C for 12 h and the yield was 88%. The next step was to synthesize ITMC monomer. In brief, under vigorous stirring, 4.8 g of ethyl chloroformate (44.0 mmol) was added into a flask containing 7.1 g of 2,2-bis(iodomethyl)-1,3-propanediol (20.0 mmol) and 100 mL of THF in an ice bath. Next, 8 mL of THF containing 4.8 g of TEA (48.0 mmol) was added dropwise to the reaction system in 2 h. Then, the ice bath was removed and the reaction was continued at room temperature for 12 h. After that, the reaction system was filtered and the collected filtrate was concentrated by rotary evaporation. The crude product obtained was purified twice via recrystallization in a mixed solvent of THF and ether (1/3, v/v). Finally, the recrystallized product was gathered and dried under vacuum at 35 °C for 24 h to obtain ITMC monomer with a yield of 56%.

4.4. Synthesis of PI

PI was synthesized by ROP of functional monomer ITMC using PEG1000 as the macroinitiator and $Zn(HMDS)_2$ as the catalyst. First, 1.0 g of PEG1000 (1 mmol) and 23 mL of anhydrous toluene were added to a 50 mL eggplant-shaped flask. Then, the residual water in the reaction system was removed by azeotropic distillation at 125 °C. Afterwards, 3.8 g ITMC (10 mmol) and 2 mL of anhydrous toluene containing 386.0 mg $Zn(HMDS)_2$ were added to the flask, and the system was stirred under a blanket of argon at 40 °C for 24 h. After the solvent was removed by a rotary evaporator, the crude product was evenly dispersed in THF and then precipitated in cold ether for 24 h. The final product was separated via dumping the supernatant and a vacuum drying was then conducted at 35 °C for another 24 h.

4.5. Synthesis of P1, P2 and P3

P1, P2 and P3 triblock copolymers were synthesized by stannous octoate-catalyzed bulk ROP of different monomers in the presence of PEG1500 as the macroinitiator [34,63]. Briefly, 15 g of PEG1500 (10 mmol) was added to a 250 mL three-necked flask, and the system was mechanically stirred at 120 °C under vacuum for 2 h to remove water from the raw materials. After that, a specified amount of monomers and stannous octoate were added to the flask at 80 °C under an argon atmosphere. After three gas substitutions, the system was in the state of argon atmosphere and heated at 150 °C for 12 h with mechanical stirring. After the completion of polymerization, heating and stirring were continued under vacuum at 120 °C for 1 h to remove unreacted monomers and low MW products. Further, the crude product was washed three times with 200 mL of water at 80 °C and then freeze-dried for about 3 days to obtain the final product.

4.6. ^1H NMR

The structures and compositions of ITMC and polymers were characterized by a 400 MHz Fourier Transform Nuclear Magnetic Resonance Spectrometer (AVANCE III HD, Bruker). All samples were dissolved in DMSO-d_6 or $CDCl_3$ to make 10 mg mL^{-1} solutions for scanning (scanning times, 16; temperature, 298 K).

4.7. GPC

The MWs and malar mass dispersity ($Đ_M$) values of synthetic specimens were confirmed using a GPC system (Agilent 1260), which equipped with a differential detector (G1362A) and a Polargel-L column (7.5 mm × 300 mm). The polymers were dissolved in chromatographic grade THF and the samples (20 μL) were then injected into the GPC system. THF was selected as the mobile phase with 1.0 mL min^{-1} flow rate at 35 °C. The standard curve was calibrated with monodisperse polystyrenes.

4.8. XPS

The surface elements of the samples were analyzed by XPS (PHI 5300). The Mg anode target ($h\nu$ = 1253.6 eV) was selected as X-ray excitation source with 250 W of power and 14 kV of voltage. Peak data were processed by software AugerScan 3.3, and the obtained binding energy spectrum peaks were corrected with C 1s peak (E_b = 284.6 eV) as the standard.

4.9. Cryo-field emission scanning electron microscopy-energy dispersion spectroscopy (Cryo-FESEM-EDS)

The surface morphology and element distributions of polymers were scanned and analyzed by a Cryo-FESEM-EDS system (AZtec X-Max Extreme EDS). Polymers were evenly spread on the sample table with conductive glue and then sprayed with a 2 nm-thickness gold coating (10 mA, 120 s) to enhance the conductivity of samples. Polymers were scanned for 2 min at 20 kV of acceleration voltage.

4.10. Preparation of aqueous polymer solutions

The preparation procedure of various aqueous polymer solutions was similar. 15% P1 and 30% PI1 aqueous solutions were prepared as examples. For 15% P1 aqueous solution, 1.5 g of P1 and 8.5 g of normal saline (NS) were added to a 25 mL vial and stirred in refrigerator at 4 °C for 3 days to obtain 15% P1 solution. As to 30% PI1 aqueous solution, 1.5 g of P1 and 7.0 g of NS were added to a 25 mL vial and stirred in refrigerator at 4 °C until the system became uniform. Then, 1.5 g of PI was added into the system and stirred at 4 °C. 2 days later, the system became uniform and 30% PI1 aqueous solution was obtained.

4.11. Dynamic rheological measurement

The rheological behaviors of the prepared aqueous polymer solutions upon heating were measured using a stress-controlled rheometer Kinexus Pro (Malvern Instrument Inc., UK). A cone plate with a diameter of 60 mm and a cone angle of 1° was selected. The distance between the upper and lower plates was set to 0.03 mm 1.5 mL of aqueous polymer solution was added dropwise on the lower plate, and a thin layer of silicone oil was covered on the edge of the cone plate to reduce the evaporation of water. Test parameters: temperature range, 15–50 °C; heating rate, 0.5 °C min^{-1}; frequency, 1.59 Hz.

4.12. In vitro Micro-CT imaging

Iohexol was diluted with deionized water to obtain a series of iohexol aqueous solutions with specified iodine content. Alumina powder and deionized water were selected as the control and blank groups, respectively. The above samples were packed into 2 mL (d = 7 mm) vials and their grayscale indices and Hounsfield units were obtained by Micro-CT (Bruker, Skyscan1176) to verify the correlation between iodine content and grayscale index/Hounsfield unit. The specific parameters used for scanning were set as follows: 1 mm aluminum filter; X-ray tube voltage, 65 kV; tube current, 370 μA; pixel space size, 35 μm; rotation step length, 0.7° s^{-1}; scanning angle range, 180°; P_{max}, 0.1. Meanwhile, 0.5 mL aqueous polymer solutions were added to 2 mL vials (d = 7 mm) and placed at 4 °C for 12 h to eliminate air bubbles generated during addition. Subsequently, Micro-CT scanning was performed to confirm the X-ray radiopacity of various aqueous polymer solutions. The grayscale indices were obtained by analyzing data with CTAn software. The specific parameters used for scanning were the same as above. The Hounsfield unit value of a system was calculated via the following equation:

$$\text{Hounsefield unit} = \frac{\mu - \mu_w}{\mu_w} \times 1000 \quad (3)$$

where μ and μ_w are the attenuation coefficients of a system and water, respectively.

4.13. "FDU" mold and imaging

A cylinder model with "FDU" pattern ($d = 30$ mm, $h = 4$ mm) was designed by the software ironCAD 2018, and the "FDU" mold made of ABS resin was then obtained by 3D printing. 0.2 mL of aqueous polymer solution was injected into the "FDU" pattern, and the surface of the mold was sealed with parafilm film to prevent water evaporation. The "FDU" mold was scanned by Micro-CT. The scanning parameters were the same as above. Meanwhile, 0.2 mL of aqueous polymer solution was injected into another "FDU" mold, and the surface of the mold was also sealed with parafilm film to prevent water volatilization. Then, the surface was further covered with different layers of 0.5 cm thick pork and scanned by X-treme (Bruker, In Vivo Xtreme). X-treme scanning parameters: X-ray resolution, 18 Ip/mm; exposure time, 1.2 s; voltage, 40 keV; filter, 0.4 mm Al; fstop, 1.1.

4.14. In vitro cytotoxicity

The *in vitro* cytotoxicity of the synthetic polymers was evaluated by CCK-8 assay. The used cell type was MC3T3-E1 cells (Shanghai Cell Bank, Chinese Academy of Sciences). First, MC3T3-E1 cells were incubated and then seeded in 96-well plates with a cell density of 5×10^3 per well. The cell culture medium containing 10% fetal bovine serum was added to the culture plate, and then cells were incubated for another 12 h to allow cells to adhere fully. Next, cell culture medium in the well plate was replaced with a fresh culture solution containing polymers with a specified concentration, and the incubation was conducted for another 24 h. Finally, the absorbance of each well at 450 nm wavelength was measured with a microplate reader (ELx808, Biotech). The cell viability of blank group that did not receive any treatment of polymers was defined as 100%. *In vitro* cytotoxicity of the sample was evaluated by the relative cell viability. Equation (4) is the calculation equation for the relative cell viability.

$$\text{viability}\ \ (\%) = \frac{\text{OD}_{\text{exp}}}{\text{OD}_{\text{blank}}} \times 100\% \tag{4}$$

where OD_{exp} and OD_{blank} are the absorbance values of the experimental and blank groups, respectively.

4.15. In vivo Micro-CT imaging

Subcutaneous injection. Female ICR mice were randomly divided into three groups, A, B, and C, with three mice in each group. Group A was injected subcutaneously with 15% P1 and 30% PI1 aqueous solutions on both sides of the spine, respectively; group B was injected subcutaneously with 15% P2 and 30% PI2 aqueous solutions, respectively; and group C was injected subcutaneously with 15% P3 and 30% PI3 aqueous solutions, respectively. The injection volume of aqueous polymer solution was 0.1 mL. Before injection, each mouse received a standard anesthesia. 30 min post-injection, all mice were scanned by Micro-CT.

4.15.1. Intraperitoneal injection

Similar to subcutaneous injection, female ICR mice were randomly divided into three groups, a, b, and c, with three mice in each group. After general anesthesia, the mice in the group a were intraperitoneally injected with 0.1 mL of 30% PI1 solution; the mice in the group b were intraperitoneally injected with 0.1 mL of 30% PI2 solution; and the mice in the group c were intraperitoneally injected with 0.1 mL of 30% PI3 solution. 30 min later, Micro-CT was used to scan all mice, and the gel volume was analyzed and calculated by 3D reconstruction. The specific parameters used for *in vivo* Micro-CT-scanning were set as follows: 1 mm aluminum filter; X-ray tube voltage, 65 kV; tube current, 370 μA; pixel space size, 35 μm; rotation step length, 0.7° s^{-1}; scanning angle range, 180°; P_{max}, 0.1.

4.16. In vivo hydrogel degradation

The mice receiving the subcutaneous injection of 30% PI1 system were subjected to Micro-CT scanning on day 0, 1, 4, 9, 14, 19, 25, and 33 post-injection, and the residual amount of gel was analyzed by 3D reconstruction. The specific parameters used for scanning were the same as *in vivo* Micro-CT scanning except P_{max} was 0.15. In addition, another 16 female ICR mice were subcutaneously injected with 15% P1 aqueous solution on both sides of the back spine and the injection volume of each site was 0.1 mL. Then, two mice were randomly euthanized and dissected on day 0, 1, 4, 9, 14, 19, 25 and 33 post-injection, and the subcutaneous residual gel was stripped and weighed for quantitative analysis.

4.17. In vivo biocompatibility

The mice treated with the 30% PI1 hydrogel were euthanized on day 49 post-injection and their heart, liver, spleen, lung kidney and subcutaneous tissues were harvested and stored in tissue fixative. All the collected tissues were embedded in paraffin, sectioned, and stained by hematoxylin-eosin (H&E). The slides were observed using an inverted microscope (Eclipse LV100ND, Nikon). The paraffin-embedded subcutaneous tissue containing the residual gel was also scanned by Micro-CT. The specific parameters used for scanning were the same as above except P_{max} was 0.25.

CRediT authorship contribution statement

Xiaohui Wu: Writing – original draft, Methodology, Investigation. **Xin Wang:** Investigation, Writing – review & editing. **Xiaobin Chen:** Investigation, Writing – review & editing. **Xiaowei Yang:** Investigation, Writing – review & editing. **Qian Ma:** Methodology. **Guohua Xu:** Funding acquisition, Validation. **Lin Yu:** Conceptualization, Funding acquisition, Supervision, Writing – review & editing. **Jiandong Ding:** Funding acquisition, Writing – review & editing.

Declaration of competing interest

There are no conflicts of interest to declare.

Acknowledgements

Authors acknowledge funding from the National Natural Science Foundation of China (grant Nos. 51773043, 81772363 and 21975045) and the National Key R&D Program of China (grant Nos. 2020YFC1107102 and 2016YFC1100300).

Appendix A. Supplementary data

Supplementary data to this article can be found online at https://doi.org/10.1016/j.bioactmat.2021.05.013.

References

[1] S.M. Janib, A.S. Moses, J.A. MacKay, Imaging and drug delivery using theranostic nanoparticles, Adv. Drug Deliv. Rev. 62 (11) (2010) 1052–1063.
[2] R. Lu, Y. Zhang, H. Tao, L. Zhou, H. Li, T. Chen, P. Zhang, Y. Lu, S. Chen, Gadolinium-hyaluronic acid nanoparticles as an efficient and safe magnetic resonance imaging contrast agent for articular cartilage injury detection, Bioact. Mater. 5 (4) (2020) 758–767.
[3] D. Li, L. Lin, Y. Fan, L. Liu, M. Shen, R. Wu, L. Du, X. Shi, Ultrasound-enhanced fluorescence imaging and chemotherapy of multidrug-resistant tumors using multifunctional dendrimer/carbon dot nanohybrids, Bioact. Mater. 6 (3) (2021) 729–739.

[4] H. Xu, B. Ma, J. Jiang, S. Xiao, R. Peng, W. Zhuang, G. Li, Y. Wang, Integrated prodrug micelles with two-photon bioimaging and pH-triggered drug delivery for cancer theranostics, Regen Biomater. 7 (2) (2020) 171–180.

[5] K. Lei, Q. Ma, L. Yu, J. Ding, Functional biomedical hydrogels for in vivo imaging, J. Mater. Chem. B 4 (48) (2016) 7793–7812.

[6] R. Samuel, E. Girard, G. Chagnon, S. Dejean, D. Favier, J. Coudane, B. Nottelet, Radiopaque poly(ε-caprolactone) as additive for X-ray imaging of temporary implantable medical devices, RSC Adv. 5 (102) (2015) 84125–84133.

[7] S. Datta, S. Jana, A. Das, A. Chakraborty, A.R. Chowdhury, P. Datta, Bioprinting of radiopaque constructs for tissue engineering and understanding degradation behavior by use of Micro-CT, Bioact. Mater. 5 (3) (2020) 569–576.

[8] J. Yin, S. Luan, Opportunities and challenges for the development of polymer-based biomaterials and medical devices, Regen Biomater. 3 (2) (2016) 129–135.

[9] D.Y. Zhao, T.T. Zhu, J. Li, L.G. Cui, Z.Y. Zhang, X.L. Zhuang, J.X. Ding, Poly(lactic-co-glycolic acid)-based composite bone-substitute materials, Bioact. Mater. 6 (2) (2021) 346–360.

[10] L. Fu, Z. Yang, C. Gao, H. Li, Z. Yuan, F. Wang, X. Sui, S. Liu, Q. Guo, Advances and prospects in biomimetic multilayered scaffolds for articular cartilage regeneration, Regen Biomater. 7 (6) (2020) 527–542.

[11] M.A. Mohamed, A. Shahini, N. Rajabian, J. Caserto, A.M.A. El-Sokkary, M.A. Akl, S.T. Andreadis, C. Cheng, Fast photocurable thiol-ene elastomers with tunable biodegradability, mechanical and surface properties enhance myoblast differentiation and contractile function, Bioact. Mater. 6 (7) (2021) 2120–2133.

[12] X. Li, X. Ji, K. Chen, M.W. Ullah, B. Li, J. Cao, L. Xiao, J. Xiao, G. Yang, Immobilized thrombin on X-ray radiopaque polyvinyl alcohol/chitosan embolic microspheres for precise localization and topical blood coagulation, Bioact. Mater. 6 (7) (2021) 2105–2119.

[13] H. Yang, K. Lei, F. Zhou, X. Yang, Q. An, W. Zhu, L. Yu, J. Ding, Injectable PEG/polyester thermogel: a new liquid embolization agent for temporary vascular interventional therapy, Mater. Sci. Eng. C Mater. Biol. Appl. 102 (2019) 606–615.

[14] J.L. Pariente, L. Bordenave, R. Bareille, C. Ohayon-Courtes, C. Baquey, M. Le Guillou, In vitro cytocompatibility of radio-opacifiers used in ureteral endoprosthesis, Biomaterials 20 (6) (1999) 523–527.

[15] C.I. Vallo, T.R. Cuadrado, P.M. Frontini, Mechanical and fracture behaviour evaluation of commercial acrylic bone cements, Polym. Int. 43 (3) (1997) 260–268.

[16] T.R. Olsen, L.L. Davis, S.E. Nicolau, C.C. Duncan, D.C. Whitehead, B.A. Van Horn, F. Alexis, Non-invasive deep tissue imaging of iodine modified poly(caprolactone-co-1-4-oxepan-1,5-dione) using X-ray, Acta Biomater. 20 (2015) 94–103.

[17] M.J. Sandker, A. Petit, E.M. Redout, M. Siebelt, B. Muller, P. Bruin, R. Meyboom, T. Vermonden, W.E. Hennink, H. Weinans, In situ forming acyl-capped PCLA-PEG-PCLA triblock copolymer based hydrogels, Biomaterials 34 (32) (2013) 8002–8011.

[18] Q. Lv, S. Yu, F. Quan, C. He, X. Chen, Thermosensitive polypeptide hydrogels Co-loaded with two anti-tumor agents to reduce multi-drug resistance and enhance local tumor treatment, Adv. Ther. 3 (3) (2020) 1900165.

[19] L.A.L. Ftiervoet, H. Zhang, E. van Groesen, K. Fortuin, N.J.C.B. Duin, K. Remaut, R. M. Schiffelers, W.E. Hennink, T. Vermonden, Local release of siRNA using polyplex-loaded thermosensitive hydrogels, Nanoscale 12 (18) (2020) 10347–10360.

[20] Q. Lv, C. He, F. Quan, S. Yu, X. Chen, DOX/IL-2/IFN-gamma co-loaded thermosensitive polypeptide hydrogel for efficient melanoma treatment, Bioact. Mater. 3 (1) (2018) 118–128.

[21] B.C. Ilochonwu, A. Urtti, W.E. Hennink, T. Vermonden, Intravitreal hydrogels for sustained release of therapeutic proteins, J. Contr. Release 326 (2020) 419–441.

[22] M. Patel, H.J. Lee, S. Park, Y. Kim, B. Jeong, Injectable thermogel for 3D culture of stem cells, Biomaterials 159 (2018) 91–107.

[23] S. Yu, C. Wang, J. Yu, J. Wang, Y. Lu, Y. Zhang, X. Zhang, Q. Hu, W. Sun, C. He, X. Chen, Z. Gu, Injectable bioresponsive gel depot for enhanced immune checkpoint blockade, Adv. Mater. 30 (28) (2018) 1801527.

[24] G. Zhong, J. Yao, X. Huang, Y. Luo, M. Wang, J. Han, F. Chen, Y. Yu, Injectable ECM hydrogel for delivery of BMSCs enabled full-thickness meniscus repair in an orthotopic rat model, Bioact. Mater. 5 (4) (2020) 871–879.

[25] Y. Zheng, G. Wu, L. Chen, Y. Zhang, Y. Luo, Y. Zheng, F. Hu, T. Forouzanfar, H. Lin, B. Liu, Neuro-regenerative imidazole-functionalized GelMA hydrogel loaded with hAMSC and SDF-1 alpha promote stem cell differentiation and repair focal brain injury, Bioact. Mater. 6 (3) (2021) 627–637.

[26] X. Ma, A. Agas, Z. Siddiqui, K. Kim, P. Iglesias-Montoro, J. Kalluru, V. Kumar, J. Haorah, Angiogenic peptide hydrogels for treatment of traumatic brain injury, Bioact. Mater. 5 (1) (2020) 124–132.

[27] Y. Wu, T. Chang, W. Chen, X. Wang, J. Li, Y. Chen, Y. Yu, Z. Shen, Q. Yu, Y. Zhang, Release of VEGF and BMP9 from injectable alginate based composite hydrogel for treatment of myocardial infarction, Bioact. Mater. 6 (2) (2021) 520–528.

[28] C. Wang, M. Wang, K. Xia, J. Wang, F. Cheng, K. Shi, L. Ying, C. Yu, H. Xu, S. Xiao, C. Liang, F. Li, B. Lei, Q. Chen, A bioactive injectable self-healing anti-inflammatory hydrogel with ultralong extracellular vesicles release synergistically enhances motor functional recovery of spinal cord injury, Bioact. Mater. 6 (8) (2021) 2523–2534.

[29] F. Cipriani, B. Arino Palao, I. Gonzalez de Torre, A. Vega Castrillo, H.J. Aguado Hernandez, M. Alonso Rodrigo, A.J. Alvarez Barcia, A. Sanchez, V. Garcia Diaz, M. Lopez Pena, J.C. Rodriguez-Cabello, An elastin-like recombinamer-based bioactive hydrogel embedded with mesenchymal stromal cells as an injectable scaffold for osteochondral repair, Regen Biomater. 6 (6) (2019) 335–347.

[30] Y. Dong, A.O. Saeed, W. Hassan, C. Keigher, Y. Zheng, H. Tai, A. Pandit, W. Wang, One-step" preparation of thiol-ene clickable PEG-based thermoresponsive hyperbranched copolymer for in situ crosslinking hybrid hydrogel, Macromol. Rapid Commun. 33 (2) (2012) 120–126.

[31] A. Petit, B. Muller, P. Bruin, R. Meyboom, M. Piest, L.M. Kroon-Batenburg, L.G. de Leede, W.E. Hennink, T. Vermonden, Modulating rheological and degradation properties of temperature-responsive gelling systems composed of blends of PCLA-PEG-PCLA triblock copolymers and their fully hexanoyl-capped derivatives, Acta Biomater. 8 (12) (2012) 4260–4267.

[32] X. Chen, J. Zhang, K. Wu, X. Wu, J. Tang, S. Cui, D. Cao, R. Liu, C. Peng, L. Yu, J. Ding, Visualizing the in vivo evolution of an injectable and thermosensitive hydrogel using tri-modal bioimaging, Small Methods 4 (9) (2020) 2000310.

[33] H.J. Lee, B. Jeong, ROS-sensitive degradable PEG-PCL-PEG micellar thermogel, Small 16 (12) (2019) 1903045.

[34] Z. Zhang, J. Ni, L. Chen, L. Yu, J.W. Xu, J.D. Ding, Biodegradable and thermoreversible PCLA-PEG-PCLA hydrogel as a barrier for prevention of post-operative adhesion, Biomaterials 32 (21) (2011) 4725–4736.

[35] X. Zhou, X. He, K. Shi, L. Yuan, Y. Yang, Q. Liu, Y. Ming, C. Yi, Z. Qian, Injectable thermosensitive hydrogel containing erlotinib-loaded hollow mesoporous silica nanoparticles as a localized drug delivery system for NSCLC therapy, Adv. Sci. 7 (23) (2020) 2001442.

[36] Y. Li, H.Y. Yang, D.S. Lee, Advances in biodegradable and injectable hydrogels for biomedical applications, J. Contr. Release 330 (2021) 151–160.

[37] X.B. Chen, M.L. Wang, X.W. Yang, Y.B. Wang, L. Yu, J. Sun, J.D. Ding, Injectable hydrogels for the sustained delivery of a HER2-targeted antibody for preventing local relapse of HER2+breast cancer after breast-conserving surgery, Theranostics 9 (21) (2019) 6080–6098.

[38] X.W. Yang, X.B. Chen, Y.B. Wang, G.H. Xu, L. Yu, J.D. Ding, Sustained release of lipophilic gemcitabine from an injectable polymeric hydrogel for synergistically enhancing tumor chemoradiotherapy, Chem. Eng. J. 396 (2020) 125320.

[39] S.J. Buwalda, T. Vermonden, W.E. Hennink, Hydrogels for therapeutic delivery: current developments and future directions, Biomacromolecules 18 (2) (2017) 316–330.

[40] H.C. Ma, C.L. He, Y.L. Cheng, D.S. Li, Y.B. Gong, J.G. Liu, H.Y. Tian, X.S. Chen, PLK1shRNA and doxorubicin co-loaded thermosensitive PLGA-PEG-PLGA hydrogels for osteosarcoma treatment, Biomaterials 35 (30) (2014) 8723–8734.

[41] F. Yang, K. Shi, Y. Hao, Y. Jia, Q. Liu, Y. Chen, M. Pan, L. Yuan, Y. Yu, Z. Qian, Cyclophosphamide loaded thermo-responsive hydrogel system synergize with a hydrogel cancer vaccine to amplify cancer immunotherapy in a prime-boost manner, Bioact. Mater. 6 (10) (2021) 3036–3048.

[42] B. Xue, M. Lei, K. Shi, M. Wang, Y. Hao, Y. Xiao, L. Yuan, J. Peng, Z. Qian, Intratumoral injection of norcantharidin-loaded poly(D, L-lactide)-b-poly(ethylene glycol)-b-Poly(D,L-lactide) thermosensitive hydrogel for the treatment of primary hepatocellular carcinoma, J. Biomed. Nanotechnol. 15 (10) (2019) 2025–2044.

[43] W.K. Xu, J.Y. Tang, Z. Yuan, C.Y. Cai, X.B. Chen, S.Q. Cui, P. Liu, L. Yu, K.Y. Cai, J. D. Ding, Accelerated cutaneous wound healing using an injectable teicoplanin-loaded PLGA-PEG-PLGA thermogel dressing, Chin. J. Polym. Sci. 37 (6) (2019) 548–559.

[44] X. Li, J. Ding, Z. Zhang, M. Yang, J. Yu, J. Wang, F. Chang, X. Chen, Kartogenin-incorporated thermogel supports stem cells for significant cartilage regeneration, ACS Appl. Mater. Interfaces 8 (8) (2016) 5148–5159.

[45] P. Ni, Q. Ding, M. Fan, J. Liao, Z. Qian, J. Luo, X. Li, F. Luo, Z. Yang, Y. Wei, Injectable thermosensitive PEG-PCL-PEG hydrogel/acellular bone matrix composite for bone regeneration in cranial defects, Biomaterials 35 (1) (2014) 236–248.

[46] K.W. Lei, Y.P. Chen, J.Y. Wang, X.C. Peng, L. Yu, J.D. Ding, Non-invasive monitoring of in vivo degradation of a radiopaque thermoreversible hydrogel and its efficacy in preventing post-operative adhesions, Acta Biomater. 55 (2017) 396–409.

[47] K. Lei, W. Shen, L. Cao, L. Yu, J. Ding, An injectable thermogel with high radiopacity, Chem. Commun. 51 (28) (2015) 6080–6083.

[48] L. Yu, G. Chang, H. Zhang, J. Ding, Temperature-induced spontaneous sol-gel transitions of poly(D,L-lactic acid-co-glycolic acid)-b-poly(ethylene glycol)-b-poly (D,L-lactic acid-co-glycolic acid) triblock copolymers and their end-capped derivatives in water, J. Polym. Sci., Part A: Polym. Chem. 45 (6) (2007) 1122–1133.

[49] L. Yu, H. Zhang, J. Ding, A subtle end-group effect on macroscopic physical gelation of triblock copolymer aqueous solutions, Angew. Chem. Int. Ed. 45 (14) (2006) 2232–2235.

[50] J.B. Luan, S.Q. Cui, J.T. Wang, W.J. Shen, L. Yu, J.D. Ding, Positional isomeric effects of coupling agents on the temperature-induced gelation of triblock copolymer aqueous solutions, Polym. Chem. 8 (17) (2017) 2586–2597.

[51] S. Cui, L. Yu, J. Ding, Thermogelling of amphiphilic block copolymers in water: ABA type versus AB or BAB type, Macromolecules 52 (10) (2019) 3697–3715.

[52] S. Cui, L. Chen, L. Yu, J. Ding, Synergism among polydispersed amphiphilic block copolymers leading to spontaneous physical hydrogelation upon heating, Macromolecules 53 (18) (2020) 7726–7739.

[53] S. El Habnouni, S. Blanquer, V. Darcos, J. Coudane, Aminated PCL-based copolymers by chemical modification of poly(α-iodo-ε-caprolactone-co-ε-caprolactone), J. Polym. Sci., Part A: Polym. Chem. 47 (22) (2009) 6104–6115.

[54] B. Nottelet, J. Coudane, M. Vert, Synthesis of an X-ray opaque biodegradable copolyester by chemical modification of poly (epsilon-caprolactone), Biomaterials 27 (28) (2006) 4948–4954.

[55] B.A. Van Horn, L.L. Davis, S.E. Nicolau, E.E. Burry, V.O. Bailey, F.D. Guerra, F. Alexis, D.C. Whitehead, Synthesis and conjugation of a triiodohydroxylamine for the preparation of highly X-ray opaque poly(ε-caprolactone) materials, J. Polym. Sci., Part A: Polym. Chem. 55 (5) (2017) 787–793.

[56] J.H. Hong, H.J. Lee, B. Jeong, Injectable polypeptide thermogel as a tissue engineering system for hepatogenic differentiation of tonsil-derived mesenchymal stem cells, ACS Appl. Mater. Interfaces 9 (13) (2017) 11568–11576.

[57] M. Patel, H.J. Lee, S. Son, H. Kim, J. Kim, B. Jeong, Iron ion-releasing polypeptide thermogel for neuronal differentiation of mesenchymal stem cells, Biomacromolecules 21 (1) (2020) 143–151.
[58] H. Lusic, M.W. Grinstaff, X-ray-computed tomography contrast agents, Chem. Rev. 113 (3) (2013) 1641–1666.
[59] K.J. Zhu, R.W. Hendren, K. Jensen, C.G. Pitt, Synthesis, properties, and biodegradation of poly(1,3-trimethylene carbonate), Macromolecules 24 (8) (1991) 1736–1740.
[60] A.-C. Albertsson, M. Eklund, Influence of molecular structure on the degradation mechanism of degradable polymers: in vitro degradation of poly(trimethylene carbonate), poly(trimethylene carbonate-co-caprolactone), and poly(adipic anhydride), J. Appl. Polym. Sci. 57 (1) (1995) 87–103.
[61] Z. Zhang, R. Kuijer, S.K. Bulstra, D.W. Grijpma, J. Feijen, The in vivo and in vitro degradation behavior of poly(trimethylene carbonate), Biomaterials 27 (9) (2006) 1741–1748.
[62] Q. Ma, K. Lei, J. Ding, L. Yu, J. Ding, Design, synthesis and ring-opening polymerization of a new iodinated carbonate monomer: a universal route towards ultrahigh radiopaque aliphatic polycarbonates, Polym. Chem. 8 (43) (2017) 6665–6674.
[63] Y. Zhuang, X. Yang, Y. Li, Y. Chen, X. Peng, L. Yu, J. Ding, Sustained release strategy designed for lixisenatide delivery to synchronously treat diabetes and associated complications, ACS Appl. Mater. Interfaces 11 (33) (2019) 29604–29618.